EURASIP Journal on Wireless Communications and Networking

RESEARCH Open Access

A flower bud-shaped flexible UWB antenna for healthcare applications

Kailash V. Karad[1,2*] and Vaibhav S. Hendre[1]

*Correspondence:
karadkv@gmail.com

[1] Department of Electronics and Telecommunication Engineering, G. H. Raisoni College of Engineering and Management, Pune 412207, India
[2] Department of Electronics and Telecommunication Engineering, GES's R. H. Sapat College of Engineering and Management Studies and Research, Nashik 422005, India

Abstract

Remote surveillance of the elderly and others with health difficulties is becoming increasingly important in these epidemic days. To address these issues, low-cost, lightweight, and portable wearable devices are in huge demand. This paper realizes the design and analysis of a flexible ultra-wideband (UWB) antenna for healthcare applications. The proposed hexagonal microstrip antenna encompasses two cuts on the top left and right side of the hexagon which looks like a flower bud. The antenna is fabricated using a flexible foam substrate with a dielectric constant of 1.07 and has a dimension of 38 × 30 × 1.7 mm^3. With a unique patch shape and corner cut in the partial ground, the present design strives to optimize the antenna structure to accommodate UWB (3.1 to 10.6 GHz) operating spectrum from 2.6 to 11.3 GHz. The proposed antenna has achieved an FBW of 125.17% with a total gain of 5.24 dB. The antenna is also evaluated on the line of bending and SAR over a tissue of 1 g and 10 g. The antenna operated admirably, with an average SAR value below the safety limits of 1.6 W/kg and 2 W/kg for the tissues, respectively.

Keywords: Bending, Flexible, Flower bud, Specific absorption rate, Ultra-wideband

1 Introduction

Wearable antennas are becoming more and more popular because of their tiny size, conformal nature, lightweight, and compactness. These antennas are in high demand in the electronics and telecom industries for usage in a variety of applications including the military, RADAR, healthcare, public safety, and many more. The Federal Communication Commission (FCC) in 2002 defined an ultra-wideband frequency with a bandwidth of 7.5 GHz, extending from 3.1 to 10.6 GHz, to be an unlicensed spectrum [1]. Similarly, for 5G communication, it is preferable to go with the existing UWB or millimeter wave (mmWave) band to enhance the requirement of bandwidth [2–4]. Although it is preferable to use the entire 7.5 GHz spectrum from UWB, the maximum power a transmitter can use is just about 0.5 mW. This is a small portion of the IEEE 802.11 a/b/g standards 2.45 GHz ISM (Industrial, Scientific, and Medical) band's capabilities. One bit of information must always be carried by combining many low-energy UWB pulses due to the extremely low transmit power that is available. In theory, increasing the number of pulses needed to carry one bit can be utilized to trade data rate for link distance. The data rate is lower and the transmission distance is higher when there are more pulses per

bit. With high data rates, this meritoriously elevates UWB to indoor, short-range communications. Wide bandwidth has led to the development of wireless UWB and personal area network applications that are designed to transport data at speeds of up to several Gbps over distances of one to ten meters [5].

In perspective to these, the features of UWB push the need for wearable antennas specifically for healthcare applications. Earlier antennas were fabricated using substrate materials like FR4, RT-duroid, etc., but it was challenging to achieve the antenna's flexibility and other desired properties. At the moment, flexible wearable antennas come in a wide range of shapes and substrates, including denim, felt, Velcro, PDMS [6], and foam [7]. The future flexible wearable antennas are likely to be based on textile material, polymers, or flexible ceramics [8–10]. The new kind of material, such as foam, which is sufficiently flexible, light, and durable and can be readily incorporated into the wearer's clothing, is the main emphasis of the antenna. The features of the following foam material types are illustrated here.

1.1 Polyurethane (PU and also called Polyester)

This well-liked family of foams is perfect for a variety of uses, including sound management in cars, air filtering in lawnmowers, and liquid delivery in medical devices. Figure 1a shows open-celled polyurethane foam which is a tough substance with outstanding cushioning and protective qualities. Specialty-controlled porosity-sized foams with higher tensile, tear, and elongation characteristics can be reticulated [11]. This foam is bouncy, similar to the foam used in pillows or mattress protectors. Given that it has open cells, the material will absorb liquids. This foam is applied to sensitive, scratch-prone parts of units such as the faces of LCD or plasma TVs and computer displays when the units being packaged are incredibly lightweight [12].

1.2 Polyethylene (PE)

Polyethylene foam gives the tough, light, closed-cell qualities required, protecting delicate electronics or giving athletic equipment comfort and support. It combines strong

(a) Polyurethane (PU) [8-9] (b) Polyethylene (PE) [9] (c) Ethylene-Vinyl Acetate (EVA) [10]

Fig. 1 Different types of foams. Three different types of foams are enlisted in **a**–**c**. **a** Open-celled polyurethane foam which is a tough substance with outstanding cushioning and protective qualities. Polyethylene foam gives the tough, light, closed-cell qualities required, protecting delicate electronics or giving athletic equipment comfort and support. It combines strong resistance to chemicals and moisture with good vibration-dampening and insulating qualities. Compared to polyurethane, this is more rigid as shown in **b**. EVA stands for ethylvinyl acetate. EVA foam refers to a closed-cell ethylvinyl acetate copolymer that is often given in the form of plates and is offered in a wide range of densities and colors as presented in **c**. Among all these types of foam as shown in this figure, EVA is the best suitable candidate from flexibility, bending, and water resistance points of view. It also makes antenna fabrication easier and more conformal

resistance to chemicals and moisture with good vibration-dampening and insulating qualities. Compared to polyurethane, this is more rigid as shown in Fig. 1b. It has characteristics that are more like those of Styrofoam but is considerably more malleable and flexible. While polyethylene foam won't split or break when bent, Styrofoam can be easily broken if bent. Due to the closed cells in polyethylene foam, liquids cannot be absorbed by it. Since it doesn't absorb liquid, this foam is popular among packaging designers and may be used to package practically any item [11, 12].

1.3 EVA foam

EVA stands for ethylvinyl acetate. EVA foam refers to a closed-cell ethylvinyl acetate copolymer that is often given in the form of plates and is offered in a wide range of densities and colors as presented in Fig. 1c. Due to its ability to be thermoformed into both simple and complex shapes, it enables us to manufacture a variety of products that are suitable for a wide range of uses [9, 10]. Copolymers of ethylene and vinyl acetate are used to create EVA (ethylene–vinyl acetate) foam. The weight percentage of vinyl acetate typically ranges from 10 to 40% in one sheet of EVA foam.

An additional crucial component for the creation of EVA foam is polyethylene material. EVA foam's density, hardness, color, durability, and other properties can vary depending on how much foaming catalysts and additives are used during the molding process. Materials made of EVA foam have a closed-cell foam structure. They offer many great qualities, such as robust heat insulation, long-term durability, superior cushioning and shock absorption, and outstanding water and moisture resistance [13].

Among all these types of foam as shown in Fig. 1, EVA is the best suitable candidate from flexibility, bending, and water resistance points of view. It also makes antenna fabrication easier and more conformal. Wearable antennas are those which can be easily worn over the body parts or the parts of clothes. Ultra-wideband systems attract research interest in implementing wireless applications. As UWB offers very low power operation [5], it has reduced the system complexity. The conventional substrate materials are not suitable for stretching, folding, or bending as it results in cracks or damage of the material directly. Also, it has increased the weight of the antenna [14].

The author [15] has implemented the wearable UWB antenna over a felt textile substrate ($\varepsilon_r = 1.2$) with a thickness of 0.7 mm resulting in an operating frequency of 3.1 GHz to 11.3 GHz. However, the overall realized gain is 4 dB. The antennas made up of textile material are bendable and can readily adjust to the curves of the human body to enhance user comfort, but they must maintain their full performance while being bent. As a result, it is important to examine the performance parameters of flexible wearable antennas under various bending conditions [16]. In [17], the author has designed and tested a wideband antenna for wearable applications using flexible jeans substrate ($\varepsilon_r = 1.8$). The antenna is operative over the frequency of 0.9 GHz to 6 GHz. A novel technique of five parallel metal plates is used for bandwidth enhancement. The author [18] designed and fabricated the antenna of size $33 \times 35\,mm^2$ using three different textile materials such as jeans, flannel, and cotton for wearable applications in the UWB frequency range. The tested antenna resulted in a maximum bandwidth of 5 GHz for the dielectric constant of 1.7 and a thickness of 1 mm. In [19], a UWB circular patch antenna for wearable application is proposed with the jeans fabric. A partial ground technique

with the two-layer substrate is incorporated into the fabrication of the antenna. The feed line is hidden with the second layer of the substrate which made the antenna function in the range of 2 GHz to 14 GHz.

The authors [20] have proposed the textile UWB antenna for biomedical communication with a dielectric as jeans (denim) material (($\varepsilon_r = 1.67$). The thickness of the dielectric substrate is taken as 2 mm, and adhesive copper tape of 0.75 mm thickness is used as conducting material. The simulated design performance analysis of the UWB antenna with FR4 and jeans substrates is carried out in [21]. However, the results are compared in terms of S_{11}, gain, and radiation pattern of two different substrates. In [22], the UWB antenna has been fabricated for breast cancer diagnosis using FR4 substrate of thickness 1. 6 mm and operates between 2 and 12 GHz. The antenna is very compact in size $28 \times 14\,mm^2$, and the SAR investigated is about 0.98 W/kg with a maximum gain of 4.2 dB. In recent literature [23], a graphene-assembled film (GAF) and a flexible ceramic substrate are used in designing of UWB antenna for wearable applications along with the co-planar waveguide feed structure of two H-shaped slots. The antenna has a size of $32 \times 52 \times 0.28\,mm^3$ with a maximum gain of 4.1 dB over the frequency range of 4.1 to 8 GHz. Also, the geometrical design of an antenna can be accomplished with pre-fractals called fractal antennas. The pre-fractal modeling has recently provided enormous versatility in engineering and applied science. These antennas are multiband with efficient miniaturization and have the properties of self-similarity and space-filling, which provide numerous benefits [24]. A fractal has a structure that is too irregular to be described by a traditional mathematical theory (Sierpinski gasket antenna). A fractal approach to modeling its geometrical configuration can be considered in order to minimize the antenna size while maintaining a high radiation efficiency along with the entropy computation based on the fractal dimension and complexity of shape [25]. The fractal geometries such as Sierpinski, Cantor, Hilbert [26], Minkowski, Koch, and the fractal tree are being used for wearable multiband and wideband applications. A hexagonal-square-shaped fractal-based approach is used to achieve the ultra-wideband in the range of frequency from 2.1 to 13.5 GHz [24, 25], 27.

Based on the literature, this research incorporates a foam-based flexible ultra-wideband antenna for healthcare applications using a partial ground approach. The substrate material is made of foam. Its small size and ability to operate in a broad frequency range of 2.6 GHz to 11.3 GHz make it the ideal material for ultra-wideband wearable applications. This paper is organized as follows. Section 1 provides an overview of foam material and related literature, Sect. 2 provides the antenna design method, Sect. 3 shows experimental work carried out, Sect. 4 includes simulated and measured findings, followed by discussion of the results, and Sects. 5, 6, and 7 provide a bending, on-body and SAR analysis followed by a conclusion in Sect. 8.

2 Method

The proposed antenna is designed by using basic hexagonal geometry. Antennas are composed of conducting materials; typically, a metal structure is used in a homogeneous medium such as air or vacuum known as free space. Metals are thought to be perfect electric conductors (PECs) [28]. Thus, a copper foil of thickness 50 microns is used as a conducting material while a foam of 1.7 mm thickness is selected as flexible

substrate. Its loss tangent ($tan\ \delta$) is 0.0025 and the dielectric constant (ε_r) is 1.07. The foam is used as the substrate because it is inexpensive, widely available, and flexible enough to blend in with the wearer's clothing. In Ansys HFSS, the theoretically designed antenna is modeled and optimized for the requirement of UWB.

2.1 Design of proposed antenna

Equations (1) to (4) defined here are used in the design of a basic structure of a hexagonal microstrip antenna [29]. Equations (2) to (4) are used in order to obtain the resonating frequency of an antenna, which is described by Eq. (1).

1. Resonating frequency:

$$f_o = \frac{c}{2(W_{\text{eff}} + 2\Delta l)\sqrt{\varepsilon_{\text{reff}}}} \tag{1}$$

where,

$$\varepsilon_{\text{reff}} = \frac{\varepsilon_r + 1}{2} + \frac{\varepsilon_r - 1}{2}\left(1 + 12\frac{h}{2W}\right)^{-1/2} \tag{2}$$

$$\Delta l = \frac{0.412h(\varepsilon_{\text{reff}} + 0.03)\left(\frac{2W}{h} + 0.258\right)}{(\varepsilon_{\text{reff}} - 0.258)\left(\frac{2W}{h} + 0.8\right)} \tag{3}$$

2. Effective width of the patch:

$$W_{\text{eff}} = W + 0.58W + 0.023\left(\sqrt{3} - 1\right) \tag{4}$$

The proposed antenna is designed with the parameters presented in Table 1. The basic hexagonal-shaped patch is cut equally from the top left and right side edges of the hexagon with 1.7 mm that has resulted in the patch being into the shape of the flower bud as shown in Fig. 2a. Also, as presented in Fig. 2b, two cuts of the size 3 mm × 4 mm at the left and right corners of the partial ground are introduced which made good enhancement in the bandwidth as well as gain of the antenna.

The proposed antenna with the partial ground has given a wideband performance (Table 2, Iteration 2). However, to enhance the gain and bandwidth, the corners of the ground structure are cut for various lengths and widths. The parametric analysis of the proposed antenna is carried out from the full ground to the cuts in corners of size 3 mm × 4 mm, and the same is depicted in Table 2. The results of these variations show enhancement in the gain as well as bandwidth parameters along with the return loss characteristic (S_{11}). The comparison of all these parameters is presented in Fig. 3.

Table 1 Proposed antenna design parameters

Parameter	L_g	W_g	L_{sub}	W_{sub}	L_f	W_f	L_1	L_2	L_3	L_{g1}	W_{g1}
Value (mm)	10	30	38	30	11	4	5	6	8	3	4

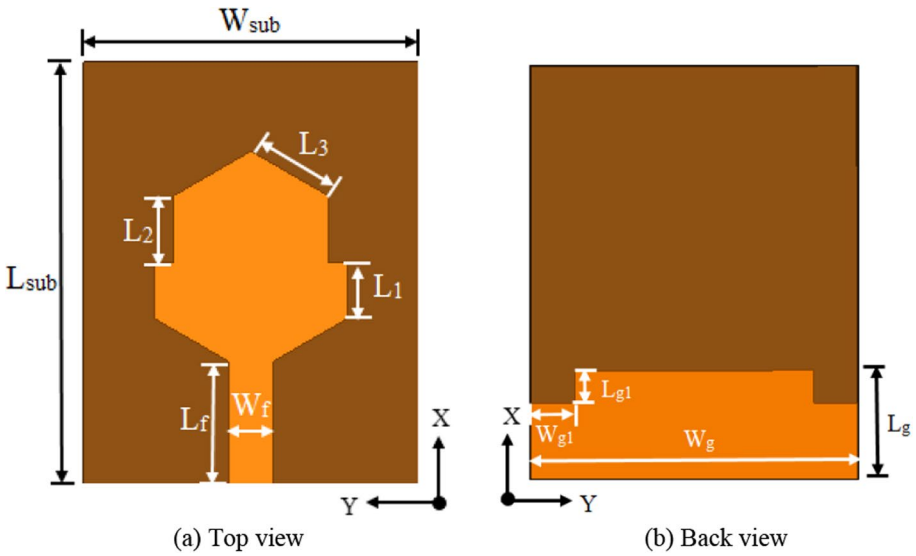

Fig. 2 Geometry of flower bud-shaped hexagonal microstrip antenna (FBHMSA). The basic hexagonal-shaped patch is cut equally from the top left and right side edges of the hexagon with 1.7 mm that has resulted in the patch being into the shape of the flower bud as shown in **a**. Also, as presented in **b**, two cuts of the size 3 mm × 4 mm at the left and right corners of the partial ground are introduced which made good enhancement in the bandwidth as well as gain of the antenna. **a**, **b** represent the top view and back view of the proposed antenna

Table 2 Parametric results with variation in the ground plane

Parameter/ geometry	Resonating at (GHz)	Bandwidth (GHz)	S_{11} (dB)	Total gain (dB)
Full ground[1] 38 mm × 30 mm	7.7	–	− 6.81	–
Partial ground[2] 10 mm × 30 mm	3.4, 6.1, 9.2	8.1	− 18.4, − 2.15, − 21.54	4.82
Corner cut[3] 3 mm × 1 mm	3.4, 6, 9.2	8.24	− 19.05, − 21.15, − 22.36	4.7
Corner cut[4] 3 mm × 2 mm	3.5, 5.8, 9.4	8.41	− 20.50.,24.16, − 22.42	4.91
Corner cut[5] 3 mm × 3 mm	3.6, 5.7, 9.6	8.45	− 21.4, − 24.42, − 20.14	5.06
Corner cut[6] 3 mm × 4 mm	3.5, 5.8, 9.8	8.70	− 21.25, − 25.58, − 18.05	5.24

According to the parametric study, the proposed antenna is resonating very well for the 3 mm × 4 mm corner cut of the partial ground plane. The antenna is resonated at three different frequencies such as 3.5, 5.8, and 9.8 GHz over the frequency of 2.60 GHz to 11.30 GHz. This band completely covers the ultra-wideband (3.1 to 10.6 GHz) frequencies and resulted in a bandwidth of 8.7 GHz. The maximum value of S_{11} (− 25.58 dB) as marked in red color is achieved at 5.8 GHz.

3 Experimental work

The simulated results of the proposed antenna are encouraging for the parameters under consideration as presented in Table 2. The dimensions of Table 1 are taken into account to fabricate the proposed antenna. The fabricated prototype of a flower bud-shaped

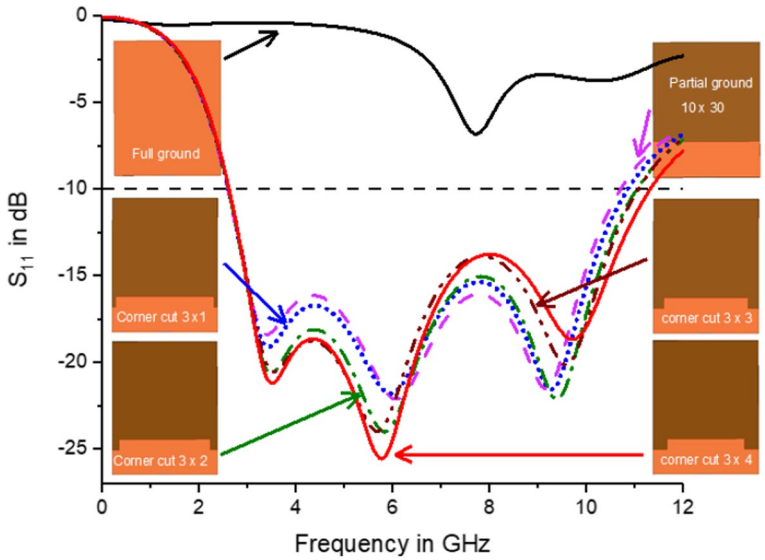

Fig. 3 Return loss (S_{11}) performance with variation in geometry of the ground structure. To enhance the gain and bandwidth, the corners of the ground structure are cut for various lengths and widths. The parametric analysis of the proposed antenna is carried out from the full ground to the cuts in corners of size 3 mm × 4 mm, and the same is depicted in Table 2. The results of these variations show enhancement in the gain as well as bandwidth parameters along with the return loss characteristic (S_{11}). The comparison of all these parameters is presented in this figure. According to the parametric study, the proposed antenna is resonating very well for the 3 mm × 4 mm corner cut of the partial ground plane. The antenna is resonated at three different frequencies such as 3.5, 5.8, and 9.8 GHz over the frequency of 2.60 GHz to 11.30 GHz. This band completely covers the ultra-wideband (3.1 to 10.6 GHz) frequencies and resulted in a bandwidth of 8.7 GHz. The maximum value of S_{11} (− 25.58 dB) as marked in red color is achieved at 5.8 GHz

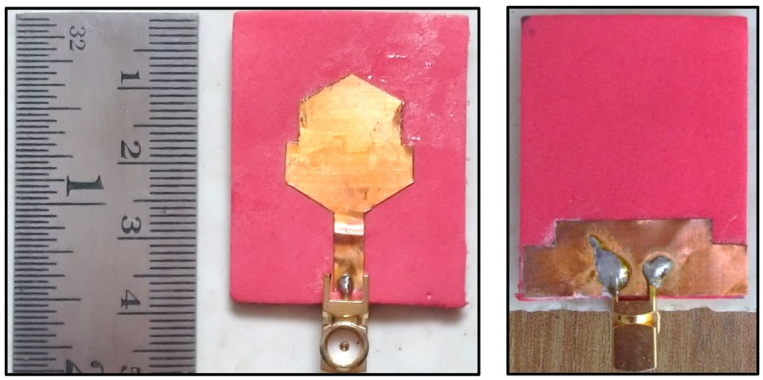

Fig. 4 Photographs of fabricated flower bud-shaped hexagonal microstrip antenna (FBHMSA). The fabricated prototype of a flower bud-shaped hexagonal microstrip antenna (FBHMSA) is made and presented in this figure. The cut at the top of the hexagon with the scale measurement represents a patch, i.e., top view of the fabricated prototype as shown in **a**, whereas **b** represents the back view as the partial ground plane

hexagonal microstrip antenna (FBHMSA) is made and presented in Fig. 4. The cut at the top of the hexagon with the scale measurement represents a patch, i.e., top view of the fabricated prototype as shown in Fig. 4a, whereas Fig. 4b represents the back view as the partial ground plane.

4 Results and discussions

The measured results are slightly skewed as compared to the simulated are shown in Fig. 5. The shifting may have been caused by the antenna's manual assembly. The discrepancies between the measured and simulated findings are attributed to minor manufacturing errors. However, little variations are perceived, and these are attributed to factors that were not taken into account in simulations, such as the SMA connectors, soldering, pasting of ground, and patch on the substrate as a tolerance in the manufacturing process.

An anechoic chamber is used to measure the antenna radiation pattern, as seen in Fig. 6. The antenna radiation is measured with the help of an anechoic chamber of size 7.5 m × 5 m × 3.3 m. The antenna is set up for far-field measurement over the distance of 5 m for the antenna under test (AUT) and the reference antenna. This anechoic chamber provides effective shielding and allows an interference-free testing environment.

A Network Analyser (Rohde and Schwarz ZVL) of 40 GHz is used in conjunction with an antenna measurement system to acquire the measured radiation patterns. Referencing the coordinate system in which the antenna is positioned (Fig. 2), the E-plane and the H-plane are considered to be the XZ plane (or phi = 0 degrees) and YZ plane (or phi = 90 degrees), respectively. Figure 7a–c depicts the simulated radiation values produced by the antenna in the E and H-planes at the frequencies of 3.5 GHz, 5.8 GHz, and 9 GHz, respectively, whereas Fig. 8a–c shows the measured radiation for the same plane at the same frequency values. At various points of radiation, there is a good agreement between the simulated and measured radiation patterns with respect to three different frequencies. At a frequency of 9 GHz, the highest gain of 5.24 dB is noted. However, at other frequencies, a slight shift in the radiation pattern is observed.

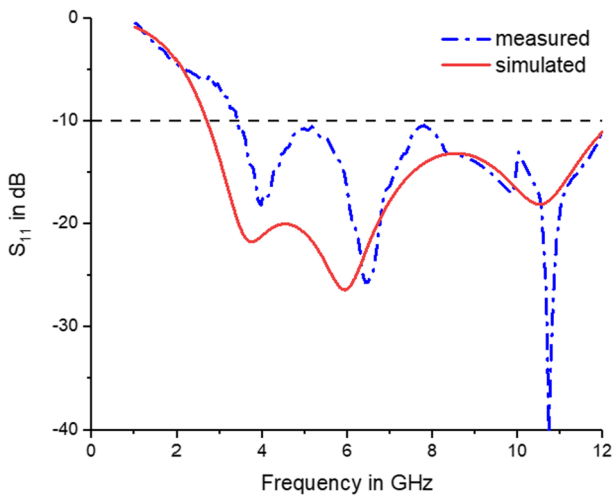

Fig. 5 Measured and simulated return loss (S_{11}). This figure represents the comparison of measured and simulated results. The measured results are slightly skewed as compared to the simulated. The shifting may have been caused by the antenna's manual assembly. The discrepancies between the measured and simulated findings are attributed to minor manufacturing errors. However, little variations are perceived, and these are attributed to factors that were not taken into account in simulations, such as the SMA connectors, soldering, pasting of ground, and patch on the substrate as a tolerance in the manufacturing process

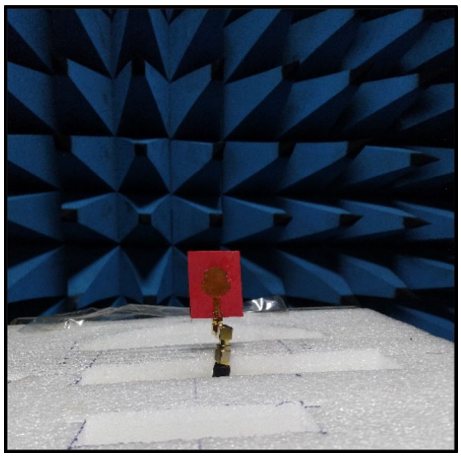

Fig. 6 Photograph of anechoic chamber set up. An anechoic chamber is used to measure the antenna radiation pattern, as seen in this figure. The antenna radiation is measured with the help of an anechoic chamber of size 7.5 m × 5 m × 3.3 m. The antenna is set up for far-field measurement over the distance of 5 m for the antenna under test (AUT) and the reference antenna. This anechoic chamber provides effective shielding and allows an interference-free testing environment

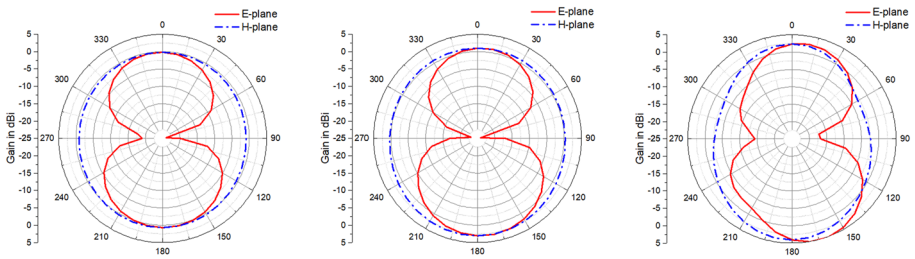

Fig. 7 E-plane and H-plane simulated radiation pattern. **a**–**c** The simulated radiation values produced by the antenna in the E and H-planes at the frequencies of 3.5 GHz, 5.8 GHz, and 9 GHz, respectively

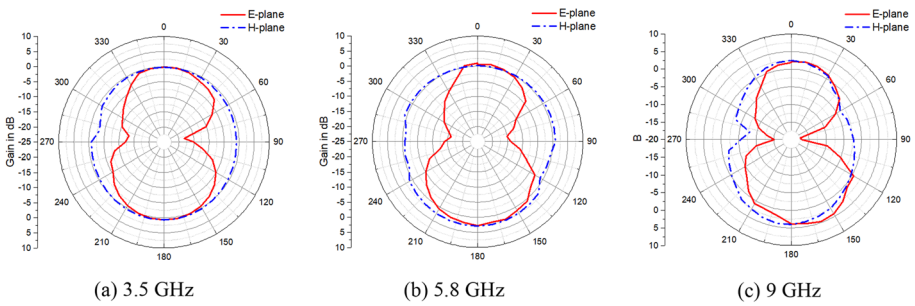

Fig. 8 E-plane and H-plane measured radiation pattern. **a**–**c** The measured radiation for the same plane at the same frequency values. At various points of radiation, there is a good agreement between the simulated and measured radiation patterns with respect to three different frequencies. At a frequency of 9 GHz, the highest gain of 5.24 dB is noted. However, at other frequencies, a slight shift in the radiation pattern is observed

The surface current distribution at 3.5 GHz, 5.8 GHz, and 9 GHz frequency is presented in Fig. 9a–c, respectively. At all the frequencies, almost a very good impedance matching is observed. At the antenna's feedline, the maximum surface current is

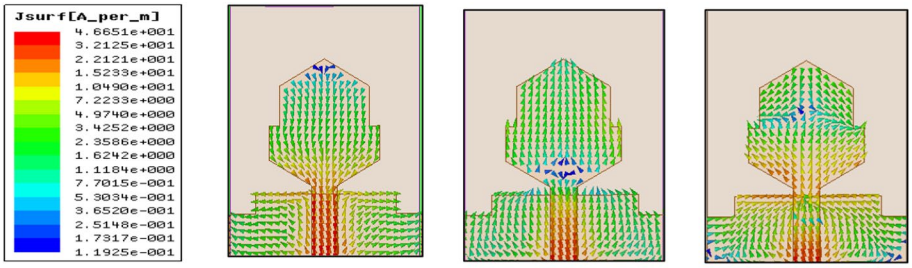

Fig. 9 Proposed antenna current distribution. The surface current distribution at 3.5 GHz, 5.8 GHz, and 9 GHz frequency is presented in **a**–**c**, respectively. At all the frequencies, almost a very good impedance matching is observed. At the antenna's feedline, the maximum surface current is 46.65 A/m. Conversely, values are lowered with the distance apart from input terminals

46.65 A/m. Conversely, values are lowered with the distance apart from input terminals. An FDTD algorithm can also be used to determine the current density over the antenna [26]. The optimization of antenna can be possibly done with wavelet expansion theory for positive definite distributions [30].

5 Bending analysis

While adjusting to the shape and movements of the human body, it is challenging to maintain the substrate's flat form [31]. Therefore, it is crucial to look into the prototype's bending performance characteristics, especially when it is worn on the arms or chest. The flexible nature of the proposed antenna is presented in Fig. 10a, b. The proposed antenna weighs 3.36 g only as shown in Fig. 10c, demonstrating both the lightweight and low-profile characteristics of the fabricated antenna. To understand the bending feasibility, the antenna is wrapped over the hollow cylindrical PVC pipe of diameter 22 mm and 48 mm as shown in Fig. 10d, e, respectively. We have investigated the S_{11} characteristics of the flexible foam at various bending diameters.

The return loss characteristic (S_{11}) plotted in Fig. 10f represents the comparison of results obtained for bending over the hollow PVC pipe of diameter 22 mm and 48 mm. The result shows a maximum value of S_{11} as -39.22 dB for bending with a small diameter; however, it gives the bandwidth of 8.47 GHz below -10 dB with a slight shift in starting frequency, whereas in the case of large diameter, it is observed that the proposed

(See figure on next page.)

Fig. 10 Bending analysis of proposed antenna at different diameters. The flexible nature of the proposed antenna is presented in **a**, **b**. The proposed antenna weighs 3.36 g only as shown in **c**, demonstrating both the lightweight and low-profile characteristics of the fabricated antenna. To understand the bending feasibility, the antenna is wrapped over the hollow cylindrical PVC pipe of diameter 22 mm and 48 mm as shown in **d**, **e**, respectively. The return loss characteristic (S_{11}) plotted in **f** represents the comparison of results obtained for bending over the hollow PVC pipe of diameter 22 mm and 48 mm. The result shows a maximum value of S_{11} as -39.22 dB for bending with a small diameter; however, it gives the bandwidth of 8.47 GHz below -10 dB with a slight shift in starting frequency, whereas in the case of large diameter, it is observed that the proposed antenna has functioned very well with a maximum value of S_{11} as -37.03 dB around 3.365 GHz and maintained the frequency response below -10 dB in the range of 2.65 GHz to 12 GHz. The response of the antenna for a smaller diameter in terms of S_{11} value is degraded to some extent when it is compared with a large diameter

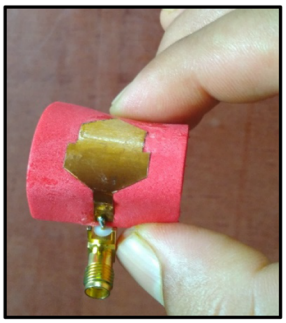

(a) Front view

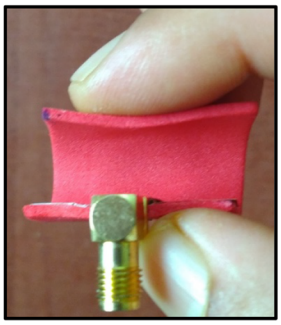

(b) Back view

(c) Weight

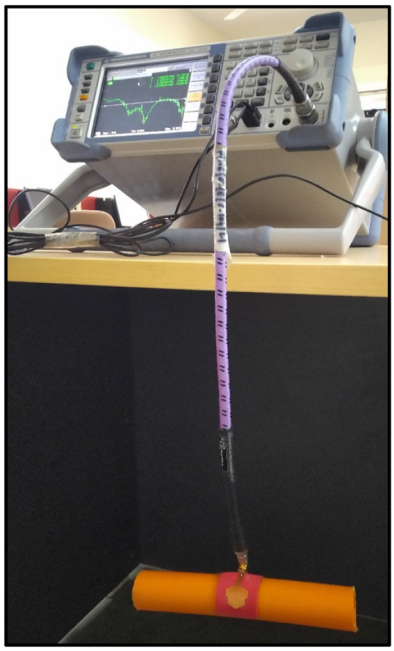

(d) Bending diameter 22 mm

(e) Bending diameter 48 mm

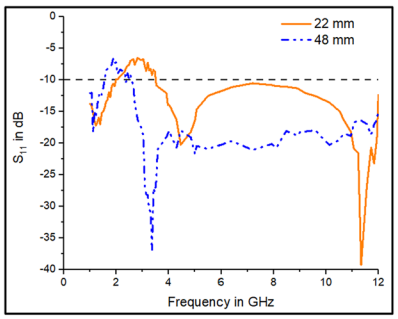

(f) Comparison of S_{11} for bending at the diameter of 22 mm and 48 mm.

Fig. 10 (See legend on previous page.)

antenna has functioned very well with a maximum value of S_{11} as -37.03 dB around 3.365 GHz and maintained the frequency response below -10 dB in the range of 2.65 GHz to 12 GHz. The response of the antenna for a smaller diameter in terms of S_{11} value is degraded to some extent when it is compared with a large diameter.

6 On-body analysis

Human tissues are lossy at higher frequencies. The electromagnetic properties of tissues have a substantial impact on various antenna parameters. When a human is nearby, antenna performance is affected [32–34] and must operate in close proximity

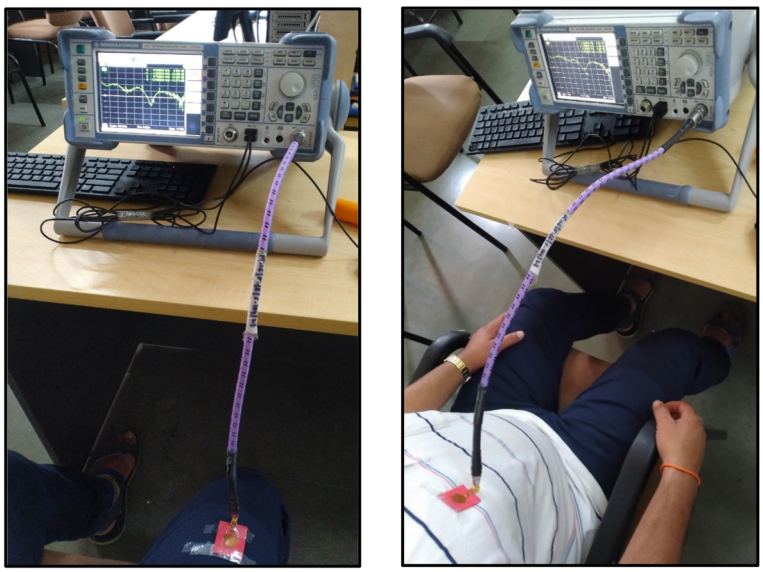

(a) leg (b) chest

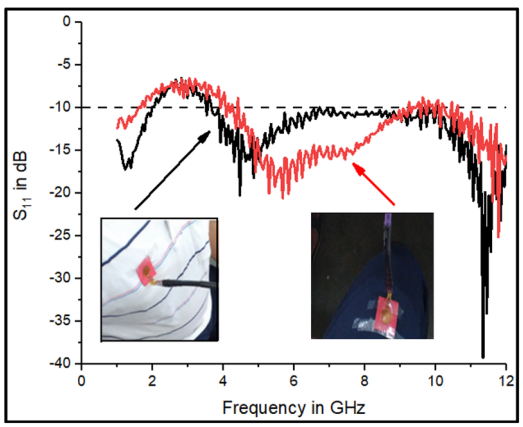

(c) comparison of measured S_{11} for chest and leg body part

Fig. 11 On-body measurements. The proposed antenna is tested for on-body performance by mounting it on the chest and leg (**a**, **b**) of the body part. The results obtained are compared and depicted in (**c**). When a human body comes into close vicinity of antenna, the performance of antenna in terms of return loss (S_{11}) and bandwidth is affected. As presented in (**c**), the response of the proposed antenna is maintained for the flat body part as the antenna is mounted on the chest. At the same time, when the antenna is tested over a curved portion of the leg, the response is affected severely in terms of bandwidth with a shift in frequency below − 10 dB

irrespective of suitable medium [35, 36]. The proposed antenna is tested for on-body performance by mounting it on the chest and leg (Fig. 11a, b) of the body part. The results obtained are compared and depicted in Fig. 11c. When a human body comes into close vicinity of antenna, the performance of antenna in terms of return loss (S_{11}) and bandwidth is affected.

As presented in Fig. 11c, the response of the proposed antenna is maintained for the flat body part as the antenna is mounted on the chest. At the same time, when the antenna is tested over a curved portion of the leg, the response is affected severely in terms of bandwidth with a shift in frequency below − 10 dB.

7 SAR analysis

Wireless devices emit radio waves, which can be absorbed by the surrounding environment, containing human beings. The penetration of radio waves in human body tissues can be measured using specific absorption rate (SAR) [37–39]. SAR is a measurement of how quickly RF energy is absorbed by our bodies when we use a wireless device. SAR is measured in Watts per kilogram (W/kg). We are continuously surrounded by many types of electromagnetic radiation in our daily lives such as Light, microwaves, cell phones, X-rays, Wi-Fi signals, and so on [40–42]. Several studies have found RF wave exposure as harmful to our health, causing tissue heating and even cell damage. SAR is created to reduce radiation exposure, as it is impossible to avoid using wireless devices fully. SAR is normally calculated as an average over the entire body or a small sample (for instance, 1 g or 10 g of tissue). The SAR value can be calculated from the electric field (E) within the bodily tissue using the formula below (when exposed to RF energy).

$$SAR = \frac{\sigma \times E^2}{\rho}$$

where SAR = specific absorption rate (in W/kg), σ = conductivity of sample (in S/m), E = electric field in RMS (in V/m), and ρ = density of sample (in kg/m^3).

A three-layer tissue equivalent phantom model is created for exploring the performance of SAR. A model for the proposed antenna is formed using electrical

Table 3 Electrical properties of human tissues

Tissue	Frequency (GHz)	Conductivity σ (S/m)	Permittivity (ε_r)	Loss tangent	Mass density (kg/m^3)
Skin (dry)	3.6	2.0855	36.92	0.28205	1109
	5.6	3.5467	35.28	0.32269	
	10	7.7869	31.484	0.45366	
Fat	3.6	0.16086	5.1641	0.15554	911
	5.6	0.28016	4.9733	0.18083	
	10	0.57091	4.6176	0.22678	
Muscle	3.6	2.6458	51.32	0.25742	1090
	5.6	4.7254	48.751	0.31114	
	10	10.337	43.035	0.44058	

parameters of the skin, fat, and muscle tissue at three frequencies 3.6, 5.8, and 10 GHz as depicted in Table 3 [43]. The three-layer body phantom of size $50 \times 50 \times 16\,mm^3$ is simulated in HFSS as shown in Fig. 12.

According to IEEE/European guidelines of the International Commission on Non-Ionizing Radiation Protection (ICNIRP), the safe threshold for 1 g of tissue is 1.6 W/kg, while the safe limit for 10 g of tissue is 2 W/kg [44–46]. The SAR analysis of the proposed antenna has been carried out on a three-layer skin, fat, and muscle tissues equivalent body phantom. The size of the phantom is taken as $50 \times 50 \times 16\,mm^3$ with 2 mm, 2 mm, and 12 mm thickness for skin, fat, and muscle layer, respectively. The SAR is investigated over 1 g and 10 g of tissues for the input power of 1 mW at three different frequencies 3.6, 5.8, and 10 GHz. Figure 13a, c, e shows the SAR values over 1 g of tissue; on the other hand, Fig. 13 b, d, f represents SAR values over 10 g of tissue.

The average values of SAR obtained are 0.0391 W/kg, 0.0819 W/kg, and 0.419 W/kg for 1 g of tissue and 0.0137 W/kg, 0.0307 W/kg, and 0.123 W/kg for 10 g of tissues. The most significant aspect of the SAR is that, even if the frequency is increased to a high level, the SAR remains below the required safety limit.

8 Conclusions

A novel flower bud-shaped UWB antenna for wearable healthcare applications has been proposed. The proposed antenna consists of a partial ground along with the flower bud-shape-type hexagonal patch over a foam substrate material. The designed antenna is compact, lightweight, cost-effective, and easily merged into the wearer's cloth as the foam material has robust heat insulation, long-term durability, superior cushioning, shock absorption, and outstanding water and moisture resistance. The overall performance of the designed antenna has been analyzed for reflection coefficient (S_{11}), gain, and bandwidth along with bending and on-body analysis. The antenna worked very well over the frequency of 2.60 to 11.30 GHz resulting in FBW of 125.17%. A total gain of 5.24 dB is reported. The measured and simulated values are found in good agreement. The antenna's ability to bend is tested using hollow PVC pipes with diameters of 22 mm and 48 mm as well as on various body parts in flat and curved positions. The results attained describe that the antenna has performed very well and attracted researchers to use foam as a flexible material.

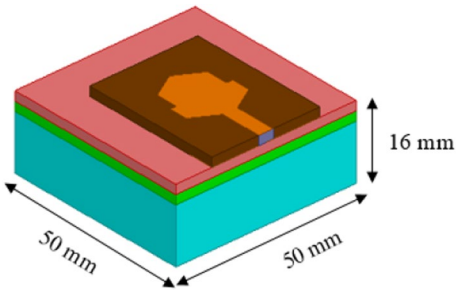

Fig. 12 Tissue equivalent three-layer phantom model. The SAR analysis of the proposed antenna has been carried out on a three-layer skin, fat, and muscle tissues equivalent body phantom. The size of the phantom is taken as $50 \times 50 \times 16\,mm^3$ with 2 mm, 2 mm, and 12 mm thickness for skin, fat, and muscle layer, respectively

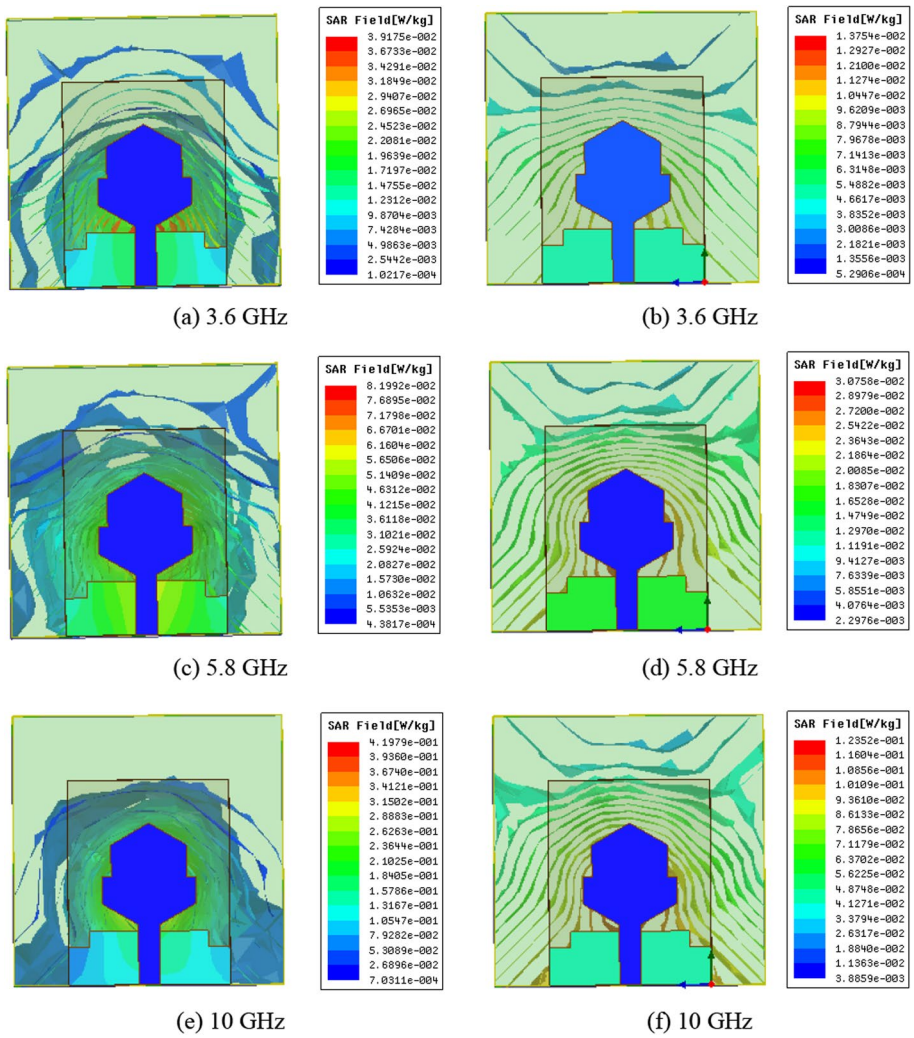

Fig. 13 SAR analysis of 1-g tissue (**a**, **c**, **e**) and 10-g tissue (**b**, **d**, **f**). The SAR is investigated over 1 g and 10 g of tissues for the input power of 1 mW at three different frequencies 3.6, 5.8, and 10 GHz. **a**, **c**, **e** show the SAR values over 1 g of tissue; on the other hand, **b**, **d**, **f** represent SAR values over 10 g of tissue. The average values of SAR obtained are 0.0391 W/kg, 0.0819 W/kg, and 0.419 W/kg for 1 g of tissue and 0.0137 W/kg, 0.0307 W/kg, and 0.123 W/kg for 10 g of tissues. The most significant aspect of the SAR is that, even if the frequency is increased to a high level, the SAR remained below the required safety limit

Abbreviations

dB	Decibel
FBW	Fractional bandwidth
E	Electric field in rms V m^{-1}
EVA	Ethylene–vinyl acetate
FR4	Fire redundant 4
GHz	Gigahertz
ICNIRP	International commission on non-ionizing radiation protection
IEEE	Institute of electrical and electronics engineers
kg	Kilogram
L	Length, in mm
LCD	Liquid crystal display
mm	Millimeter
PDMS	Polydimethylsiloxane
SAR	Specific absorption rate
S	Scattering

TV	Television
UWB	Ultra-wideband
W	Width, in mm
σ	Conductivity of sample, S m^{-1}
ε	Permittivity
ρ	Density of sample kg m^{-3}
1	Length 1
S_{11}	Return loss
L_2	Length 2
L_3	Length 3
g	Ground
g_1	Partial ground
f	Feed
r	Relative
sub	Substrate

Acknowledgements
The authors are thankful to the R. V. College of Engineering, Bengaluru, and PICT College of Engineering Pune, India, for an anechoic chamber and testing facility at the Centre of Excellence.

Author contributions
KVK designed, fabricated, and tested the antenna and also arranged and simulated models required for antenna performance under different tests. VSH analyzed and interpreted the data for plotting the results of antenna performance under various conditions such as bending, on-body, and SAR analysis. Both authors read and approved the final manuscript.

Authors' information
Kailash V. Karad received his bachelor's degree in Electronics and Telecommunication from SRES College of Engineering, Kopargaon, SPPU, Pune, in 2007 and master's degree from SSGBCOET, Bhusawal, North Maharashtra University, in 2013 and pursuing PhD degree from G. H. Raisoni College of Engineering and Management, Pune, under SPPU, Pune. He is presently working as an Assistant Professor at GES's R. H. Sapat College of Engineering, Nashik in Electronics and Telecommunication Engineering department. His research interest lies in the field of electrical networks, electromagnetics and transmission lines, antenna and wave propagation, antenna array and mobile communication.
Dr. Vaibhav S. Hendre received his B.E. (Electronics and Telecommunication Engineering) from University of Pune and M. Tech. in Electronics and Telecommunication from Dr. Babasaheb Ambedkar Technological University, Lonere, in 2006. He received his PhD from Satyabhama University, Chennai-600119, Tamil Nadu, India. He is currently serving as Deputy Director and Professor of the Department of Electronics and Telecommunication Engineering, G H Raisoni College of Engineering and Management, Savitribai Phule Pune University, Pune-411048, Maharashtra, India. Having 23 years of academic experience, his fields of interest are error control coding, MIMO systems in wireless digital communications and cognitive communication. He is a member of IEEE Communication Society and Life Member of ISTE.

Funding
The authors declare that they have not received any grant or funding for this research work by state, national or international agency, institute and or industry.

Availability of data and materials
The datasets generated and/or analyzed during the current study are not publicly available due to research work but are available from the corresponding author on reasonable request.

Declarations

Competing interests
The authors declare that they have no competing interests.

Received: 16 January 2023 Accepted: 5 March 2023
Published online: 10 March 2023

References

1. Revision of Part 15 of the Commission's Rules Regarding Ultra Wideband Transmission Systems. First Report and Order, Technical Report. ET Docket 98-153, FCC 02-48, Federal Communications Commission (2002)
2. K.V. Karad, V.S. Hendre, Design and Simulation of 28 GHz antenna for 5G mmWave communication, in *ICCCE 2021. Lecture Notes in Electrical Engineering*, vol. 828, ed. by A. Kumar, S. Mozar (Springer, Singapore, 2022)
3. J. Hatte, V. Hendre, Dwindle coupled loop antenna system for 5G communication applications. J. Commun. Technol. Electron. **66**(Suppl 2), S100–S108 (2021)
4. K.V. Karad, V.S. Hendre, Review of Antenna Array for 5G Technology Using mmWave Massive MIMO, in *Recent Trends in Electronics and Communication. Lecture Notes in Electrical Engineering*, vol. 777, ed. by A. Dhawan, V.S. Tripathi, K.V. Arya, K. Naik (Springer, Singapore, 2022)
5. I. Oppermann, M. Hamalainen, J. Iinatti, *UWB Theory and Applications* (Wiley, New York, 2004)

6. S.N. Mahmood, A.J. Ishak, T. Saeidi, H. Alsariera, S. Alani, A. Ismail, A.C. Soh, Recent advances in wearable antenna technologies: a review. Prog. Electromagn. Res. B **89**, 1–27 (2020)
7. K.V. Karad, V.S. Hendre, A foam-based compact flexible wideband antenna for healthcare applications. Prog. Electromagn. Res. C **123**, 197–212 (2022)
8. A.G. Al-Sehemi, A.A. Al-Ghamdi, N.T. Dishovsky, N.T. Atanasov, G.L. Atanasova, Design and performance analysis of dual-band wearable compact low-profile antenna for body-centric wireless communication. Int. J. Microw. Wirel. Technol. **10**, 1–11 (2018)
9. A. ElAttaoui, M. Hazmi, A. Jilbab, A. Bourouhou, Wearable wireless sensors network for ECG telemonitoring using neural network for features extraction. Wirel. Presonal Commun. **111**, 1–22 (2019)
10. G. Atanasova, N. Atanasov, Small antennas for wearable sensor networks: impact of the electromagnetic properties of the textiles on antenna performance. Sensors **20**(18), 5157 (2020)
11. https://casescases.com/foam-types
12. https://www.ufpt.com/materials/foam
13. https://www.foamtechchina.com/eva-foam-material
14. B.B.Q. Elias et al., Bandwidth optimization of a textile PIFA with DGS using characteristic mode analysis. Sensors **21**(7), 2516 (2021)
15. M. El Gharbi et al., Novel ultra-wide band wearable antenna under different bending conditions for electronic-textile applications. J. Text. Inst. **112**(3), 437–443 (2021)
16. M.F. Ismail, M.K.A. Rahim, M.R. Hamid, H.A. Majid, Bending analysis on circular polarization array textile antenna, in *2014 IEEE Asia-Pacific Conference on Applied Electromagnetics (APACE)*, pp. 139–141 (2014)
17. F. Khajeh-Khalili, Y. Khosravi, A novel wearable wideband antenna for application in wireless medical communication systems with jeans substrate. J. Text. Inst. **112**(8), 1266–1272 (2021)
18. S. Amit, V. Talasila, P. Shastry, A semi-circular slot textile antenna for ultra wideband applications, in *2019 IEEE International Symposium on Antennas and Propagation and USNC-URSI Radio Science Meeting*, pp. 249–250 (2019)
19. M.A.R. Osman, M.K.A. Rahim, M. Azfar. A., K. Kamardin, F. Zubir, N.A. Samsuri, Design and analysis UWB wearable textile antenna, in *Proceedings of the 5th European Conference on Antennas and Propagation (EUCAP)*, pp. 530–533 (2011)
20. S. Parameswari, C. Chitra, Compact textile UWB antenna with hexagonal for biomedical communication. J. Ambient Intell. Humaniz. Comput. (2021)
21. D. Mohan, C.D. Suriyakala, Ergonomics of textile antenna for body-centric wireless networks for UWB application, in *International Conference on Circuit, Power and Computing Technologies (ICCPCT)*, Kollam, pp. 1–8
22. S. Sadasivam, B.V. Thulasi, *A Compact Diamond Shaped Ultra-Wide Band Antenna System for Diagnosing Breast Cance*. Technology and Health Care Pre-press, pp 1–12 (2022)
23. R. Fang et al., Compact and low-profile UWB antenna based on graphene-assembled films for wearable applications. Sensors **20**(9), 2552 (2020)
24. E. Guariglia, Harmonic Sierpinski gasket and applications. Entropy **20**, 714 (2018)
25. E. Guariglia, Entropy and fractal antennas. Entropy **18**(3), 84 (2016)
26. C. Puente, J. Romeu, R. Pous, A. Cardama, On the behavior of the Sierpinski multiband fractal antenna. IEEE Trans. Antennas Propag. **46**(4), 517–524 (1998)
27. R. Kumar, R. Sinha, A. Choubey, SK Mahto (2021) An ultrawide band monopole antenna using hexagonal-square shaped fractal geometry. J. Electromagn. Waves Appl. **35**(2), 233–244 (2021)
28. F.P. Andriulli, A. Tabacco, G. Vecchi, A multiresolution approach to the electric field integral equation in antenna problems. SIAM J. Sci. Comput. **29**(1), 1–21 (2007)
29. K.P. Ray, M.D. Pandey, Resonance frequency of hexagonal and half hexagonal Microstrip antennas. Microw. Opt. Technol. Lett. **51**(2), 448–452 (2009)
30. E. Guariglia, *Fractional-Wavelet Analysis of Positive Definite Distributions and Wavelets on D′(C)* (Springer, Berlin, 2016)
31. S. Sankaralingam, B. Gupta, Development of textile antennas for body wearable applications and investigations on their performance under bent conditions. Prog. Electromagn. Res. B **22**, 53–71 (2010)
32. B. Prudhvi Nadh, B.T.P. Madhav, M. Siva Kumar, M. Venkateswara Rao, T. Anilkumar, Int. J. RF Microwave Comput. Aided Eng. **29**(4), 1–15 (2019)
33. P. Ranjan, S. Raj, G. Upadhyay, S. Tripathi, V.S. Tripathi, Circularly slotted flower shaped UWB filtering antenna with high peak gain performance. AEU-Int. J. Electron. Commun. **81**, 209–217 (2017)
34. L. Liu, S.W. Cheung, R. Azim, M.T. Islam, A compact circular-ring antenna for ultra-wideband applications. Microw. Opt. Technol. Lett. **53**(10), 2283–2288 (2011)
35. U. Ali et al., Design and SAR analysis of wearable antenna on various parts of human body, using conventional and artifcial ground planes. J. Electr. Eng. Technol. **2**(1), 317–328 (2017)
36. M.D. Sharma, A. Yadav, S. Singhal, R. Sharma, Performance investigation of flexible UWB antenna near human body for wearable appliances. Prog. Electromagn. Res. B **97**, 131–147 (2022)
37. A.M. Ali, M.A. Al Ghamdi, M.M. Iqbal et al., Next-generation UWB antennas gadgets for human health care using SAR. J. Wirel. Commun. Netw. **2021**, 33 (2021)
38. S. Jayakumar, G. Mohanbabu, A wearable low profile asymmetrical slotted ultra-wide band antenna for WBAN applications. J. Wirel. Commun. Netw. **2022**, 103 (2022)
39. S. Parameswari, C. Chitra, Textile UWB antenna with metamaterial for healthcare monitoring. Int. J. Antennas Propag. **2021**, 5855626 (2021)
40. https://www.everythingrf.com/community/what-is-sar
41. K. Varshini, T.R. Rao, Investigations on SAR and thermal effects of a body wearable microstrip antenna. Wirel. Pers. Commun. **96**, 3385–3401 (2017)
42. K. Varshini, T.R. Rao, Estimation of specific absorption rate using infrared thermography for the biocompatibility of wearable wireless devices. Prog. Electromagn. Res. M **56**, 101–109 (2017)

43. P.A. Hasgall, F. Di Gennaro, C. Baumgartner, E. Neufeld, B. Lloyd, M.C. Gosselin, D. Payne, A. Klingenb¨ock, N. Kuster, IT'IS Database for thermal and electromagnetic parameters of biological tissues, Version 4.1 (2022)
44. S. Doddipalli, A. Kothari, P. Peshwe, A low profile ultrawide band monopole antenna for wearable applications. Int. J. Antennas Propag. **2017**, 7362431 (2017)
45. S.J. Priyadarshini, D.J. Hemanth, Investigation and reduction methods of specific absorption rate for biomedical applications: a survey. Int. J. RF Microw. Comput. Aided Eng. **28**(3), 1–15 (2018)
46. J.P. Stephen, D.J. Hemanth, An investigation on specific absorption rate reduction materials with human tissue cube for biomedical applications. Int. J. of RF Microw. Comput.-Aided Eng. **29**(12), e21960 (2019)

Publisher's Note